physica status solidi pss rrl
www.pss-rapid.com

Local Structure of $Ga_{85:8}In_{14:2}$ Eutectic Alloy and Its Pressure–Temperature Melting Line

Yimin Mijiti, Angela Trapananti, Lucie Nataf, Francois Baudelet, Toru Shinmei, Tetsuo Irifune, Jian Zhong Jiang, and Andrea Di Cicco**

The structure of the $Ga_{85.8}In_{14.2}$ eutectic liquid alloy is investigated both under ambient conditions and at high pressure/high temperature using X-ray absorption spectroscopy (XAS) and X-ray diffraction (XRD) techniques. The local structure of the liquid alloy at ambient conditions is analyzed using double-edge refinements of the XAS data. Solid–liquid phase transitions under high-pressure and high-temperature conditions are monitored by combined XAS and XRD measurements along several quasi-isobaric heating runs, allowing to draw a melting line up to 10 GPa. The established melting line is found to be slightly below the one of pure gallium (Ga) and to follow its trend as expected from the eutectic nature of the compound. A series of Ga *K*-edge X-ray absorption fine structure (XAFS) spectra measured at different pressures indicates the absence of large structural modifications at local Ga sites in the liquid within the investigated pressure and temperature range.

1. Introduction

Gallium (Ga) and several of its alloys are liquid metals at or near room temperature. The eutectic Ga–In alloy of composition $Ga_{85.8}In_{14.2}$ has a melting point $T \approx 15\,^{\circ}C$ at ambient pressure.[1] With their special electrical, thermal, mechanical, fluidic, and surface properties, eutectic Ga–In alloys receive significant attention for their potential for various advanced applications.[2] For example, being liquid with metallic conductivity and low viscosity, Ga–In alloys can be useful for stretchable or shape reconfigurable electronics.[3] Liquid Ga–In alloys with many metals adhere to most surfaces to form ohmic contacts. When exposed to air, GaIn forms a thin "skin" composite of gallium oxide, improving its mechanical stability.[4] Unlike mercury (Hg) that is widely used as a liquid metal at ambient conditions, Ga–In alloys have low-level toxicity and reduce the safety concerns in the laboratory environments or in applications spaces. As a result, there are increasing number of studies on Ga–In systems that investigate their possible applications for techniques including functional electronics, flexible devices, 3D printing, transformable liquid metal nanomedicine, and self-healing circuits.[2,3,5–8]

Apart from the research in the direction of applied sciences, the Ga–In alloy also received attention in recent years as an interesting system for studying the structure of metallic melts under extreme conditions, thanks to its easily accessible liquid phase in a wide pressure range. Understanding the phase behavior of metallic liquids including crystallization, vitrification, and liquid–liquid transitions has important implications in fundamental and applied science.[9–13] In particular, occurrence of polyamorphism (liquid–liquid or amorphous–amorphous phase transitions) in metallic liquids and glasses is an intriguing phenomenon with limited but growing number of experimental evidences in recent years.[13–17] The nature of such transitions in liquids is still a matter of debate and needs further clarifications.

Experimental studies on polyamorphism are often conducted on low-melting-point metals such as Ga, Bi, Rb, Cs, and Sn due to their easily accessible liquid phases at high pressure and their peculiar short-range liquid structures.[14,15,18–20] The $Ga_{85.8}In_{14.2}$ (GaIn) eutectic alloy ($T_m = 288.3$ K) has been recently investigated in this context.[21–25] Recent X-ray diffraction (XRD) experiments and theoretical simulations conducted by some of us on GaIn have shown liquid-to-crystal transition and further

Y. Mijiti, A. Trapananti, A. Di Cicco
Physics Division
School of Science and Technology
University of Camerino
Via Madonna delle Carceri 9, Camerino, MC 62032, Italy
E-mail: emin.mijiti@unicam.it; andrea.dicicco@unicam.it

Y. Mijiti, L. Nataf, F. Baudelet
Synchrotron Soleil
L'Orme des Merisiers BP 48, Gif-sur-Yvette 91192, Cedex, France

T. Shinmei, T. Irifune
Geodynamics Research Center
Ehime University
Matsuyama 790-8577, Japan

J. Z. Jiang
International Center for New-Structured Materials (ICNSM)
Laboratory of New-Structured Materials
State Key Laboratory of Silicon Materials, and School of Materials Science and Engineering
Zhejiang University
Hangzhou 310027, P. R. China

The ORCID identification number(s) for the author(s) of this article can be found under https://doi.org/10.1002/pssr.202100423.

DOI: 10.1002/pssr.202100423

crystalline polymorphism under pressure, as well as indications of liquid polyamorphism under increasing temperature.[21–23] Even though a tentative phase diagram has been presented,[23] the melting curve of the alloy is not yet well established with only two experimental data points up to 10 GPa. Moreover, the local structural parameters of these promising materials have not been reported in detail even for ambient conditions.

In this work, we first studied the local structure of the liquid alloy using double-edge refinements of X-ray absorption spectroscopy (XAS) data measured at the Ga and In *K*-edges. We have also carried out systematic measurements at various pressures up to 10 GPa using a combination of two complementary techniques: energy-dispersive XAS and XRD. Both XAS and XRD experiments are able to identify the occurrence of solid–liquid phase transitions, providing also important information on the local atomic structure. The main purpose of this work is to characterize the liquid local structure and establish a reliable melting curve of this GaIn alloy in this pressure range for which signs of an anomalous behavior of the liquid are expected.

2. XAFS Analysis at Ambient Conditions

XAFS data for the as-prepared alloys were analyzed using GNXAS[26,27] data analysis method, based on multiple-scattering simulations and an advanced structural refinement using nonlinear fitting of the raw absorption data. Ga and In *K*-edge XAFS analysis of the elemental Ga and In liquids was presented in previous publications (see[28–31] respectively), where relevant details can be found. For the GaIn eutectic alloy, the multiple-edge XAFS refinement capabilities of GNXAS,[27,32] allowed a simultaneous fitting of the Ga and In *K*-edge data.

As shown in **Figure 1** and **2**, the near-edge parts of the Ga *K*-edge XAS and extended x-ray absorption fine structure (EXAFS) oscillations from GaIn liquid and pure Ga are quite similar, whereas the In *K*-edge XAS and EXAFS signals of eutectic GaIn show some distinct differences with the corresponding spectra of the elemental liquid In. These differences are due to the presence of Ga atoms (the majority species for this composition) in the neighborhood of In in the alloy. XAFS analysis was conducted accounting for the Ga–Ga, Ga–In, and In–In distance distributions, modeled as asymmetric *Γ*-like peaks as expected for a liquid system (see other studies[27,30] and refs. therein). In this case, each distribution function depends on four structural parameters, related to the coordination number *N*, average bond distance *R*, variance σ^2, and a dimensionless skewness parameter β of each first-neighbor peak (Ga–Ga and In–Ga/Ga–In and In–In). Coordination numbers of the

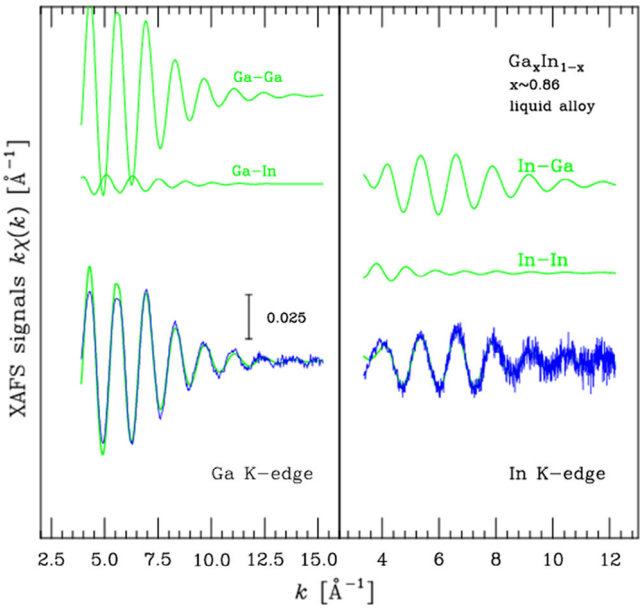

Figure 2. Best-fit XAFS refinement of the GaIn eutectic liquid alloy. Left panel: Ga *K*-edge XAFS experimental data (blue curve), compared with the calculated signals (green curves) accounting for Ga–Ga and Ga–In distance distributions (individual signals are shown in the upper part). Right-hand panel: In *K*-edge XAFS experimental data (blue curve), compared with the calculated signals (green curves) accounting for In–Ga and In–In distance distributions (individual signals are shown in the upper part).

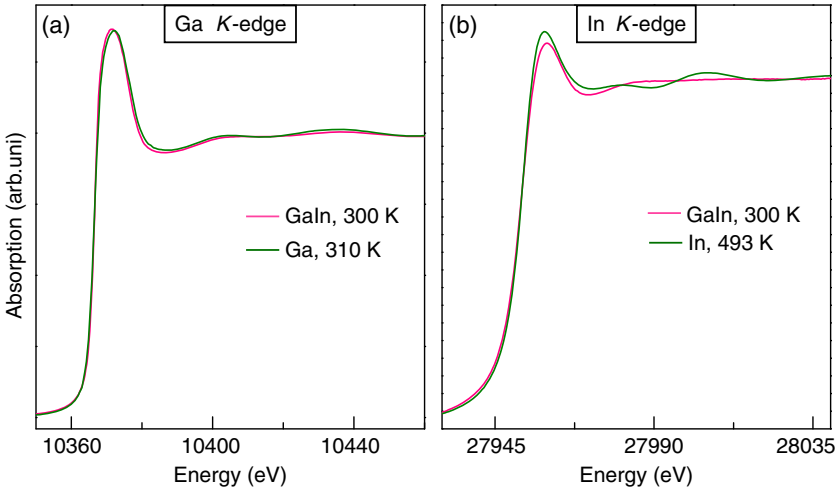

Figure 1. a) Ga and b) In *K*-edge XANES data of GaIn eutectic liquid alloy are compared with the reference spectra of liquid Ga ($T = 310$ K) and liquid In ($T = 493$ K).

individual distributions were constrained to the known stoichiometry ($x \approx 0.86$) so that $N_{GaGa} = N_{InGa} = N \times x$ and $N_{GaIn} = N_{InIn} = N \times (1 - x)$, where N was varied in the range known for liquid Ga (8-10). Distance, variance, and skewness of the Ga–In and In–Ga distance distributions were obviously constrained to be the same. Therefore, a total number of ten structural parameters (three sets of R, σ^2, and β values and the total coordination number N) was used in the double-edge refinement process.

The results are shown in Figure 2, clearly showing that simple first-neighbor distribution modeling nicely reproduces the measured XAFS experimental data. The Ga *K*-edge and In *K*-edge XAFS spectra are dominated by the Ga–Ga and In–Ga signals, respectively, as expected due to the larger abundance of Ga atoms ($x \approx 0.86$). The best-fit structural parameters were also found to be very reasonable, in line with previous results obtained in pure Ga and In.[28–30,33] The total coordination number was $N = 8.0$ (5); the average distances $R_{GaGa} = 2.84$ (1) Å, $R_{GaIn} = 3.12$ (2) Å, and $R_{InIn} = 3.27$ (5) Å; the distance variances $\sigma^2_{GaGa} = 0.032$Å^2, $\sigma^2_{GaIn} = 0.043$Å^2, and $\sigma^2_{InIn} = 0.060$Å^2 (typical uncertainties on σ^2 were 10%), whereas skewness was found to be $\beta \approx 0.8$ for the three distributions (typical 20% uncertainty).

These results are consistent with the local structure of a random liquid alloy, without formation of fragments or nuclei with different compositions (In rich or Ga rich).

3. High-Pressure Experiments: Results and Discussion

XRD is one of the most widely used techniques for the measuring the solid–liquid boundaries under extreme conditions. The onset of melting in the XRD data is often associated with the disappearance of sharp diffraction peaks of the solid or with appearance of diffusive scattering signals from the liquid. In contrast, XAS is also very sensitive to subtle changes in the structure and can be efficiently used for detection of phase transitions. A specific technique (single-energy X-ray absorption detection) has been proposed and widely used at energy-scanning beamlines[34,35] to monitor temperature-induced phase transitions at a given pressure from changes of the absorption at fixed energy. This technique was also applied to high-pressure energy-dispersive XAS data (see also ref. [30]) and in recent years has been also proposed as an efficient and convenient alternative technique for detecting the melting of metals under high pressure and high temperature (see refs. [18–20,36]). Changes of specific edge features or damping of the oscillations upon heating have been also used for monitoring melting in several elemental transition metals including Fe, Ni, and Co and their alloys.[37–41] In addition, sensitivity to the valence states and element selectivity of the technique have been found to be very useful for detecting chemical reactions that may occur in experiments involving the molten samples under extreme pressure and temperature.[41]

Combined XAS and XRD data were collected in this study at different temperatures along compression and quasi-isobaric heating runs, as shown in **Figure 3**. Each Ga *K*-edge XAS spectra (labeled by Latin letters from a to w) in (A), (B), (C), and (D) one by one corresponds to the XRD data in (E), (F), (G), and (H), respectively. Pressure and temperature values of each data point were indicated, together with the experimental paths (shown with arrows) on the T versus P phase diagram shown in **Figure 4**. As shown in Figure 3A, line shape of the main absorption peak (≈10 370 eV) and higher-energy oscillations of the initial XAS data (labeled by a) are similar to the Ga *K*-edge XAS spectrum of the elemental liquid Ga at near-ambient conditions (see Figure 1). As mentioned in the previous section, this is not surprising, as the local structure of Ga sites in the GaIn eutectic alloy resembles the one of elemental liquid Ga and is not altered at this initial pressure. Because of the liquid character, XRD data (line a and b) at the initial pressures have no sharp diffraction peaks, except those associated with the nano-polycrystalline diamond (NPD) anvils and Re gasket, as shown in Figure 3E.

The sample was compressed initially without heating until observing the crystallization through the appearance of a sharp diffraction peak at about 3.5 GPa. This new peak that appeared at $q \approx 2.35$Å^{-1} can be indexed to the (101) planes of the known *C*-centered monoclinic structure of GaIn.[21] Other relatively weak diffraction peaks were not observed because of the limited angular range in the used experimental geometry[42] and also due to the low statistics in the number and orientation of the crystalline grains (e.g., compared with the fine powder samples). Noticeably, oscillatory features after the white line peak of the XAS spectra in Figure 3A (spectra: c) become more evident upon crystallization, being compatible with the increased structural order.

After crystallization at 3.5 GPa, the diamond anvil cell (DAC) was heated, maintaining a constant membrane pressure but measuring the sample pressure before and after each XAS/XRD data collection. Combined XAS and XRD data were measured at four different temperature points along this first heating run up to 338 K, as shown in Figure 3A,E. As might be expected, the new peak around ≈2.35Å^{-1} in the XRD data (Figure 3E), which was associated above the crystalline GaIn, became almost undetectable upon heating at 328 K ($P = 4.35$ GPa, partial melting) and disappeared completely at 338 K ($P = 4.68$ GPa, melting), indicating crystal-to-liquid phase transition. Correspondingly, the XAS features that gained intensity upon crystallization becomes less evident again at 328 and 338 K (see spectra e and f in Figure 3A). Such spectral evolution is very similar to the previously observed changes in the Ga *K*-edge XAS data across the solid–liquid transitions in the confined Gallium droplets,[35] Thus, the damping of the XAFS oscillations upon heating during this experiments can be regarded as an additional evidence of melting, complementing the corresponding XRD data (blue lines e and f in Figure 3E).

Following the experimental path, which is shown in Figure 4, three other quasi-isobaric heating cycles were conducted starting at 5.0, 7.4, and 9.5 GPa. As shown in Figure 3B:D, 3F:H, combined XRD and XAS data were collected at different temperatures, along these quasi-isobaric heating runs until reaching the liquid (or almost completely melted) phase. As it was also observed in the previous standard XRD (isothermal) experiment,[23] intensity of the diffraction peak associated with the sample varies along the heating runs. This can be possibly attributed to the random rotation of few (compared with the fine powder samples) crystals which are formed by compression/cooling in these experiments. Looking at the disappearance of the (101) peak in the XRD data and modifications in the XAS

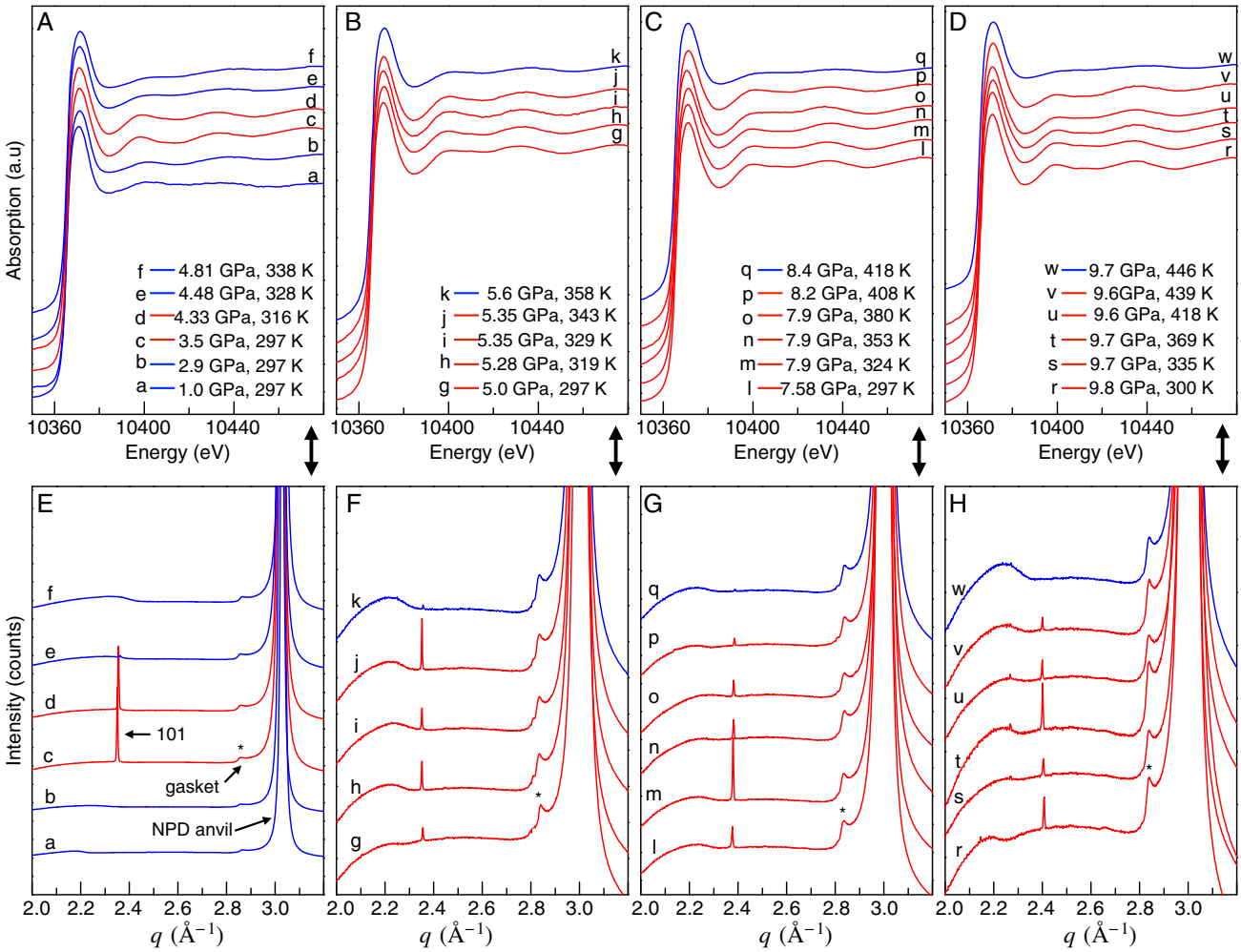

Figure 3. A–H) Combined XAS (A–D) and XRD (E–H) data at various thermodynamic conditions up to 9.5 GPa and 446 K. Data measured in the solid phase are plotted with red lines, whereas the data measured in the liquid phases are plotted with blue lines. Each Ga *K*-edge XAS spectra (labeled by Latin letters from a to w) in (A), (B), (C), and (D) one by one correspond to the XRD data in (E), (F), (G), and (H), respectively.

spectra (as discussed earlier), melting (or quasicomplete) transitions were observed at three other temperatures: 358 K ($P = 5.46$ GPa), 418 K ($P = 8.2$ GPa), and 446 K ($P = 9.5$ GPa). As soon as diffraction peaks were found to disappear in the recorded 2D diffraction images, measurements were not carried out at higher temperature in the liquid phase to be cautious for possible chemical reactions between the molten sample and the metallic gasket. A deeper analysis (after the integration of the 2D images) reaveled a minor fraction of residual solid phase at some pressure (represented by half-filled points in Figure 4) at which the sample can be therefore considered almost completely melted, with a residual crystalline phase.

As a result, six melting (or quasicomplete melting) data points (represented by filled or half-filled points in Figure 4) can be determined, allowing us to draw a tentative melting line of the liquid alloy for the 3.0–10 GPa pressure range, as shown in Figure 4. Melting points obtained in this work are slightly below the known melting line of pure Ga, as expected from the eutectic nature of the GaIn alloy. The melting line has the same trend with pressure as for elemental Ga.

The near-edge region of the Ga *K*-edge XAS spectra, measured within the molten (or partially molten) phase (indicated by blue stars in Figure 4), is shown in **Figure 5**. We can see that the XAS spectra at all experimental conditions (slightly above the melting line) are similar, suggesting similar structural arrangements at the local Ga sites. This may imply the absence of significant modifications in the liquid structure within the investigated pressure and temperature ranges, although slight structural changes cannot be excluded just from this qualitative analysis. Similarity of the XAS spectra at the initial and final data points shows that no chemical reactions or sample modifications occurred during the entire experiment. In contrast, the nearly linear trend of the melting line also supports this conclusion, as formation of a sample other than $Ga_{85.8}In_{14.2}$ with different chemical compositions or eutectic concentrations may affect the melting temperatures. Further experiments and data analysis allowing a complete quantitative and double-edge refinement of the EXAFS data in the whole pressure range is foreseen and will be the subject of a dedicated forthcoming paper.

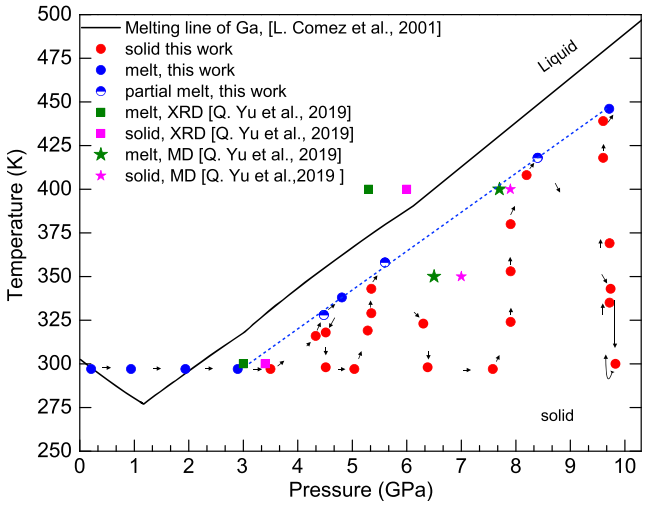

Figure 4. Experimental conditions of the combined XAS and XRD data in Figure 3 were mapped onto the *T* versus *P* phase diagram. The red dots (•) represent the thermodynamic conditions in the solid phase, whereas the blue dots (•) represent the data points in the liquid phase. The black curve (—) is the melting line of elemental Ga,[52] whereas the blue dashed line (- - -) represents a linear fit of the melting line of the eutectic GaIn established in the present study. The data points represented by other colors and shapes are from the isothermal XRD experiments of *Q*. See the study by Yu et al,[23] to compare different results. The experimental path is indicated by black arrows (→).

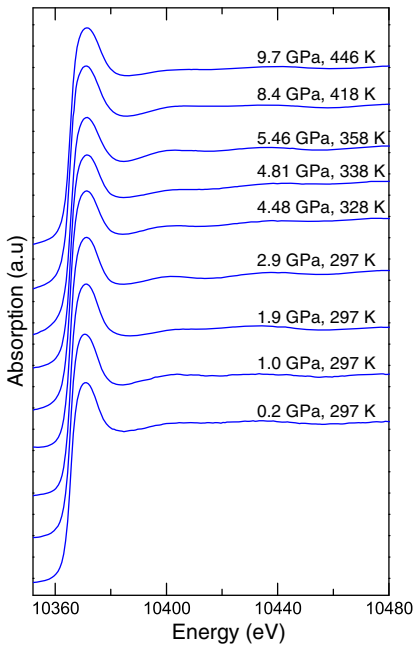

Figure 5. Ga *K*-edge XANES of GaIn in the liquid phase at several *P* and *T* conditions slightly above the established melting line (labeled by blue dots) in Figure 4.

In summary, the structure of the $Ga_{85.8}In_{14.2}$ eutectic liquid alloy has been investigated under ambient and high-pressure high-temperature conditions using XAS and XRD techniques. At first, the liquid structure at ambient conditions was studied in detail using double-edge XAS refinements. However, the structures of the eutectic liquid alloy under high-pressure and high-temperature conditions were studied using combined XAS and XRD measurements. Melting transitions were simultaneously monitored from both techniques along several quasi-isobaric heating runs, allowing us to draw a melting line up to 10 GPa. Features of the Ga *K*-edge XAS data indicate the absence of significant structural modifications at the local Ga sites in the liquid within the investigated pressure and temperature range.

4. Experimental Section

The liquid $Ga_{85.8}In_{14.2}$ (GaIn) eutectic alloy was prepared with high-purity Ga (99.99%) and In (99.99%) and characterized using X-ray techniques under ambient conditions. Ga and In *K*-edge XAS spectra at ambient pressure and room temperature were measured at the energy-scanning XAFS beamline[43] of Elettra Synchrotron (Trieste, Italy) and at the SAMBA beamline[44] of Soleil synchrotron (Saclay, France), respectively. The sample for Ga *K*-edge measurements collected in the transmission mode was prepared using procedures successfully applied for previous XAS experiments on pure liquid Ga and Hg,[45] as a fine emulsion of metal liquid droplets in epoxy resin. The sample used for In *K*-edge EXAFS measurements, collected in fluorescence mode, was instead a thin $Ga_{85.8}In_{14.2}$ liquid layer spread on a glass substrate. Combined XAS and XRD data under high-pressure and high-temperature conditions were collected at the ODE beamline of Synchrotron SOLEIL using the setup described in detail in other studies.[42,46] The energy-dispersive photon beam was focused at the sample region with an elliptically curved Si (111) crystal. X-ray absorption at different energies was simultaneously measured by a position-sensitive charge coupled device (CCD) detector. The pixel-to-energy calibration of the Ga *K*-edge XAS data was conducted using the *K*-edge XAS spectrum of a Ga_2O_3 reference sample, previously measured under ambient conditions in the energy scanning mode. Angle-dispersive XRD data were recorded using a MAR345 area detector placed on an off-axis position with respect to the beam and a quasimonochromatic beam ($E \approx 10350$ eV) selected by a slit aperture (see the study by Coppari et al. for more detail). For high-pressure XAS experiments, an appropriate quantity of GaIn liquid sample was loaded into a 120 μm hole of a preindented Re gasket without any pressure medium but together with several tiny pieces of ruby and $Sm^{2+}:SrB_4O_7$ pressure markers. The sample was then pressurized using a membrane diamond anvil cell equipped with nano-polycrystalline diamond anvils[47,48] and heated with an external resistive heater. Temperature was finely controlled and stabilized using a proportional integral derivative (PID) temperature control system and measured through the back side of the diamond anvil using a type-*K* thermocouple, with a typical ≈ 3 K accuracy. Pressure was measured using the pressure-dependent fluorescence line shift of $Sm^{2+}:SrB_4O_7$[49] and also checked by the ruby fluorescence line shift.[50,51]

Acknowledgements

The authors thank Alain Polian and Jean Coquet for their precious help with high-pressure experiments. The authors kindly acknowledge Emiliano Fonda, Andra Zitolo, and Giuliana Aquilanti for EXAFS measurements of the as-prepared alloy specimens at Soleil and Elettra synchrotrons, respectively. The authors acknowledge Synchrotron SOLEIL for beam time at the ODE beamline. Y.M. thanks the CRUI foundation for the postdoc grant. J.Z.J acknowledges financial support from NNSFC (11975202). The authors also acknowledge the support of PRIUS project (no. 2019-B37) by the Joint Usage/Research Center PRIUS, Ehime University, Japan. The authors thank Sergey V. Rashchenko at the

Sobolev Institute of Geology and Mineralogy for providing Sm:SrB4O7 pressure calibrants.

Open Access Funding provided by Universita degli Studi di Camerino within the CRUI-CARE Agreement.

Conflict of Interest

The authors declare no conflict of interest.

Data Availability Statement

The data that support the findings of this study are available from the corresponding author upon reasonable request.

Keywords

GaIn eutectic liquid, melting lines, phase transitions, structures

Received: August 2, 2021
Revised: September 11, 2021
Published online: October 19, 2021

[1] B. C. Rugg, T. G. Chart, *CALPHAD* **1990**, *14*, 115.
[2] G. Bo, L. Ren, X. Xu, Y. Du, S. Dou, *Adv. Phys.: X* **2018**, *3*, 1446359.
[3] Y. Zheng, Z. He, Y. Gao, J. Liu, *Sci. Rep.* **2013**, *3*, 1786.
[4] M. D. Dickey, R. C. Chiechi, R. J. Larsen, E. A. Weiss, D. A. Weitz, G. M. Whitesides, *Adv. Funct. Mater.* **2008**, *18*, 1097.
[5] G. Schwartz, B. C.-K. Tee, J. Mei, A. L. Appleton, D. H. Kim, H. Wang, Z. Bao, *Nat. Commun.* **2013**, *4*, 1859.
[6] C. Ladd, J.-H. So, J. Muth, M. D. Dickey, *Adv. Mater.* **2013**, *25*, 5081.
[7] Y. Lu, Q. Hu, Y. Lin, D. B. Pacardo, C. Wang, W. Sun, F. S. Ligler, M. D. Dickey, Z. Gu, *Nat. Commun.* **2015**, *6*, 10066.
[8] E. J. Markvicka, M. D. Bartlett, X. Huang, C. Majidi, *Nat. Mater.* **2018**, *17*, 618.
[9] Y. Sun, H. Song, F. Zhang, L. Yang, Z. Ye, M. I. Mendelev, C.-Z. Wang, K.-M. Ho, *Phys. Rev. Lett.* **2018**, *120*, 085703.
[10] M. Bhat, V. Molinero, E. Soignard, V. Solomon, S. Sastry, J. Yarger, C. Angell, *Nature* **2007**, *448*, 787.
[11] S. Ding, Y. Liu, Y. Li, Z. Liu, S. Sohn, F. J. Walker, J. Schroers, *Nat. Mater.* **2014**, *13*, 494.
[12] L. Zhong, J. Wang, H. Sheng, Z. Zhang, S. X. Mao, *Nature* **2014**, *512*, 177.
[13] S. Wei, F. Yang, J. Bednarcik, I. Kaban, O. Shuleshova, A. Meyer, R. Busch, *Nat. Commun.* **2013**, *4*, 2083.
[14] F. A. Gorelli, S. De Panfilis, T. Bryk, L. Ulivi, G. Garbarino, P. Parisiades, M. Santoro, *J. Phys. Chem. Lett.* **2018**, *9*, 2909.
[15] S. Falconi, L. F. Lundegaard, C. Hejny, M. I. McMahon, *Phys. Rev. Lett.* **2005**, *94*, 125507.
[16] H. Sheng, H. Liu, Y. Cheng, J. Wen, P. Lee, W. Luo, S. Shastri, E. Ma, *Nat. Mater.* **2007**, *6*, 192.
[17] Q.-S. Zeng, Y. Ding, W. L. Mao, W. Yang, S. V. Sinogeikin, J. Shu, H.-K. Mao, J. Z. Jiang, *Phys. Rev. Lett.* **2010**, *104*, 105702.
[18] R. Poloni, S. De Panfilis, A. Di Cicco, G. Pratesi, E. Principi, A. Trapananti, A. Filipponi, *Phys. Rev. B* **2005**, *71*, 184111.
[19] A. Di Cicco, A. Trapananti, E. Principi, S. De Panfilis, A. Filipponi, *Appl. Phys. Lett.* **2006**, *89*, 221912.
[20] E. Principi, M. Minicucci, A. Di Cicco, A. Trapananti, S. De Panfilis, R. Poloni, *Phys. Rev. B* **2006**, *74*, 064101.
[21] Q. Yu, A. S. Ahmad, K. Ståhl, X. D. Wang, Y. Su, K. Glazyrin, H. P. Liermann, H. Franz, Q. P. Cao, D. Zhang, J. Z. Jiang, *Sci. Rep.* **2017**, *7*, 1139.
[22] Q. Yu, X. Wang, Y. Su, Q. Cao, Y. Ren, D. Zhang, J. Jiang, *Phys. Rev. B* **2017**, *95*, 224203.
[23] Q. Yu, Y. Su, X. Wang, K. Ståhl, K. Glazyrin, H. Liermann, H. Franz, Q. Cao, D. Zhang, J. Jiang, *J. Appl. Phys.* **2019**, *126*, 015902.
[24] D. Nefedov, D. Podorozhkin, E. Charnaya, A. Uskov, J. Haase, Y. Kumzerov, A. Fokin, *J. Phys.: Condens. Matter* **2019**, *31*, 255101.
[25] Q. Yu, F. Guo, X. Wang, K. Ståhl, Y. Ren, Q. Cao, D. Zhang, J. Jiang, *J. Mol. Liq.* **2019**, *293*, 111464.
[26] A. Filipponi, A. Di Cicco, C. R. Natoli, *Phys. Rev. B* **1995**, *52*, 15122.
[27] A. Filipponi, A. Di Cicco, *TASK Quart.* **2000**, *4*, 575.
[28] A. Di Cicco, A. Filipponi, *J. Non-Cryst. Solids* **1993**, *156*, 102.
[29] A. Di Cicco, A. Filipponi, *Europhys. Lett.* **1994**, *27*, 407.
[30] L. Comez, A. Di Cicco, J.-P. Itié, A. Polian, *Phys. Rev. B* **2002**, *65*, 014114.
[31] A. Filipponi, A. Di Cicco, S. De Panfilis, A. Trapananti, J.-P. Itié, M. Borowski, S. Ansell, *J. Synchrotron Radiat.* **2001**, *8*, 81.
[32] A. Di Cicco, *Phys. Rev. B* **1996**, *53*, 6174.
[33] Y. Waseda, *The Structure of Non-Crystalline Materials*, McGraw-Hill, New York **1980**.
[34] A. Filipponi, M. Borowski, P. W. Loeffen, S. De Panfilis, A. Di Cicco, F. Sperandini, M. Minicucci, M. Giorgetti, *J. Phys.: Condens. Matter* **1998**, *10*, 235.
[35] A. Di Cicco, *Phys. Rev. Lett.* **1998**, *81*, 2942.
[36] M. Minicucci, A. Trapananti, A. Di Cicco, S. De Panfilis, G. Aquilanti, *Phys. Scr.* **2005**, *2005*, 1056.
[37] G. Aquilanti, A. Trapananti, A. Karandikar, I. Kantor, C. Marini, O. Mathon, S. Pascarelli, R. Boehler, *Proc. Natl. Acad. Sci. USA* **2015**, *112*, 12042.
[38] S. Boccato, R. Torchio, I. Kantor, G. Morard, S. Anzellini, R. Giampaoli, R. Briggs, A. Smareglia, T. Irifune, S. Pascarelli, *J. Geophys. Res.: Solid Earth* **2017**, *122*, 9921.
[39] S. Boccato, R. Torchio, S. Anzellini, E. Boulard, F. Guyot, T. Irifune, M. Harmand, I. Kantor, F. Miozzi, P. Parisiades, A. D. Rosa, D. Antonangeli, G. Morard, *Sci. Rep.* **2020**, *10*, 11663.
[40] R. Torchio, S. Boccato, F. Miozzi, A. Rosa, N. Ishimatsu, I. Kantor, N. Sévelin-Radiguet, R. Briggs, C. Meneghini, T. Irifune, G. Morard, *Geophys. Res. Lett.* **2020**, *47*, e2020GL088169.
[41] G. Morard, S. Boccato, A. D. Rosa, S. Anzellini, F. Miozzi, L. Henry, G. Garbarino, M. Mezouar, M. Harmand, F. Guyot, E. Boulard, I. Kantor, T. Irifune, R. Torchio, *Geophys. Res. Lett.* **2018**, *45*, 11.
[42] F. Coppari, A. Di Cicco, E. Principi, A. Trapananti, N. Pinto, A. Polian, S. Chagnot, A. Congeduti, *High Pressure Res.* **2010**, *30*, 28.
[43] A. Di Cicco, G. Aquilanti, M. Minicucci, E. Principi, N. Novello, A. Cognigni, L. Olivi, *J. Phys.: Conf. Ser.* **2009**, *190*, 012043.
[44] S. Belin, V. Briois, A. Traverse, M. Idir, T. Moreno, M. Ribbens, *Phys. Scr.* **2005**, *2005*, 980.
[45] L. Ottaviano, A. Filipponi, A. Di Cicco, *Phys. Rev. B* **1994**, *49*, 11749.
[46] F. Baudelet, Q. Kong, L. Nataf, J. Cafun, A. Congeduti, A. Monza, S. Chagnot, J. Itié, *High Pressure Res.* **2011**, *31*, 136.
[47] T. Irifune, A. Kurio, S. Sakamoto, T. Inoue, H. Sumiya, *Nature* **2003**, *421*, 599.
[48] N. Ishimatsu, N. Kawamura, M. Mizumaki, H. Maruyama, H. Sumiya, T. Irifune, *High Pressure Res.* **2016**, *36*, 381.
[49] S. V. Rashchenko, A. Kurnosov, L. Dubrovinsky, K. D. Litasov, *J. Appl. Phys.* **2015**, *117*, 145902.
[50] A. Dewaele, M. Torrent, P. Loubeyre, M. Mezouar, *Phys. Rev. B* **2008**, *78*, 104102.
[51] F. Datchi, A. Dewaele, P. Loubeyre, R. Letoullec, Y. Le Godec, B. Canny, *High Pressure Res.* **2007**, *27*, 447.
[52] L. Comez, A. Di Cicco, J. P. Itié, A. Polian, *Phys. Rev. B* **2001**, *65*, 014114.